

# Toward a concordance teleparallel Cosmology I: Background Dynamics

---

Mahmoud Hashim, Waleed El Hanafy,<sup>1</sup> Alexey Golovnev and Amr El-Zant

*Centre for Theoretical Physics, The British University in Egypt, P.O. Box 43, El Sherouk City, Cairo 11837, Egypt*

*E-mail:* [mahmoud@aims.ac.za](mailto:mahmoud@aims.ac.za), [waleed.elhanafy@bue.edu.eg](mailto:waleed.elhanafy@bue.edu.eg),  
[alexey.golovnev@bue.edu.eg](mailto:alexey.golovnev@bue.edu.eg), [amr.elzant@bue.edu.eg](mailto:amr.elzant@bue.edu.eg)

ABSTRACT: Assuming the universe to be spatially flat with homogeneous and isotropic background, we study the cosmological viability of the infrared corrected  $f(T) = Te^{\beta T_0/T}$  teleparallel gravity in terms of its background expansion history, including its effect on the linear growth of matter perturbations. As the dimensionless parameter  $\beta$  is completely constrained by the current density parameter, this theory does not introduce extra free parameters. This novel feature renders the theory statistically comparable on equal footing with  $\Lambda$ CDM, which is not common with modified gravity based cosmological models. Using recent cosmological observations — Pantheon supernova Type Ia, Hubble constant  $H_0$ , Baryon acoustic oscillation, redshift space distortions, Big Bang nucleosynthesis and the cosmic microwave background constraint on the decoupling acoustic scale — the joint likelihood analysis of the  $f(T)$  gravity shows very good agreement with data to within  $1\sigma$ . It explains late acceleration by weakening gravity on cosmological distances rather introducing dark energy. Although the exponential infrared  $f(T)$  gravity and  $\Lambda$ CDM are physically different, they are phenomenologically and statistically equivalent. However, the former shows more flexibility in fitting accurately determined observational constraints while decreasing the  $H_0$  tension without worsening the  $S_8$  tension. This calls for further examination of the empirical viability of the theory at the linear perturbation level, which is the subject of paper II.

KEYWORDS: Cosmological parameters–Modified gravity

---

<sup>1</sup>Corresponding author.

---

## Contents

<b>1</b>	<b>Introduction</b>	<b>1</b>
<b>2</b>	<b><math>f(T)</math> cosmology</b>	<b>3</b>
2.1	$f(T)$ modification of the background dynamics	5
2.2	$f(T)$ modification of growth function	6
<b>3</b>	<b>The exponential IR <math>f(T)</math> model</b>	<b>7</b>
<b>4</b>	<b>Observational constraints and datasets</b>	<b>9</b>
4.1	Astronomical datasets	10
4.1.1	Supernovae type Ia	10
4.1.2	$H_0$ measurements	10
4.1.3	Baryon acoustic oscillation	10
4.1.4	Redshift-space distortion	11
4.2	Cosmological constraints and allowed parameter space	11
4.2.1	BBN constraint on Baryon density	11
4.2.2	CMB constraints	11
4.2.3	Parameter space	12
<b>5</b>	<b>Results</b>	<b>12</b>
5.1	Viability of the $f(T)$ -CDM model	12
5.2	Consistency with observations	14
5.3	The Hubble constant	15
5.4	Amplitude of the growth of structure	17
<b>6</b>	<b>Conclusion</b>	<b>19</b>

---

## 1 Introduction

Cosmological observations of Supernovae Type Ia (SNIa) distances embodied the first direct evidence for a shift from cosmic deceleration to acceleration a few billion years ago [1, 2]. This phenomenon can be accounted for through the introduction of a dark energy (DE) component, with negative pressure, into Friedmann equation. The simplest description invokes a cosmological constant  $\Lambda$ , with an equation of state (EoS) fixed to  $w_{DE} = -1$ , into the field equations of general relativity (GR). Adding this to a pressureless cold dark matter (CDM) component defines the dark sector of the  $\Lambda$ CDM model. Although the model suffers theoretical problems, such as fine tuning [3, 4], it precisely fits a variety of cosmological and astrophysical observations. The simplicity and empirical success of  $\Lambda$ CDM has lead to its

wide acceptance, fundamental problems regarding the origin of the cosmological constant notwithstanding.

However, recent observations with unprecedented accuracy provide some evidences of possible physics beyond  $\Lambda$ CDM. A major problem involves the current value of the Hubble parameter  $H_0$ . The cosmic microwave background (CMB) observations by Planck (base- $\Lambda$ CDM) infer  $H_0 = 67.4 \pm 0.5$  km/s/Mpc [5], while its most recent value according to direct local measurements is  $H_0 = 74.0 \pm 1.4$  km/s/Mpc [6], which is about  $4.4\sigma$  away from Planck (see also [7–9]).

The  $H_0$  value inferred by Planck, assuming  $\Lambda$ CDM, is supported by an independent dataset that combines the baryon acoustic oscillation (BAO) and big bang nucleosynthesis (BBN) with clustering and weak lensing from the Dark Energy Survey (DES) [10]. On the other hand, the late universe measurement by SH0ES is supported by non distance ladder methods [11, 12]. And the same conclusion has been achieved by using anchors other than Cepheids to calibrate the SNIa distance ladder [13, 14]. In general, the tension between the early and the late universe of the  $H_0$  measurements is at the  $4\sigma$ –to– $6\sigma$  level for different combinations of datasets ([15], see also [16]).

The amplitude of matter fluctuations,  $\sigma_8$ , also provide another evidence of tension between the early and the late universe measurements, which is often referred to as  $S_8 \equiv \sigma_8 \sqrt{\Omega_m/0.3}$  tension. The CMB measurements imply  $S_8 = 0.834 \pm 0.016$  [5], as inferred by Planck base- $\Lambda$ CDM. On the other hand, cosmic shear base- $\Lambda$ CDM observations from late the universe give  $S_8 = 0.745 \pm 0.039$  (as measured by Kilo Degree Survey (KiDs-450) [17]); and  $S_8 = 0.737^{+0.040}_{-0.036}$  (as measured by KiDs+VIKING-450 [18]) which are about  $2$ – $2.3\sigma$  lower than Planck. The preference for  $\sigma_8$  values lower than Planck are obtained using redshift space distortion (RSD) observations [19, 20].

One may interpret the  $H_0$  tension as a discrepancy in two measurements. One (early universe) measure involves the sound horizon at radiation drag  $r_{drag}$ . This being the case, one may resort to changes in early universe physics to ease the tension by reducing the sound horizon [21–24]. However, it has been shown that classical extensions of  $\Lambda$ CDM — such as allowing for more parameters by varying the number and masses of neutrinos — do not solve the  $H_0$  tension on their own. They also worsen the  $\sigma_8$  tension ([5], see also [25]). On the other hand, in the extended 12 parameter space, when a dark energy equation of state  $w < -1$  and neutrino species other than the standard ones are allowed to vary simultaneously, there is no preference for increasing  $N_{eff}$  when  $H_0$  tension is addressed [26–28]. Self interacting neutrinos provide a better framework for solving both tensions simultaneously. But the tightly-coupled neutrinos scenario, unlike free streaming, does not phase shift the photon-baryon fluctuations. Hence, the CMB power spectra are slightly displaced towards high- $\ell$ , and the acoustic scale  $\theta_s$  at recombination must take larger values in order to restore the fit with observed CMB. It remains a challenge to construct and verify viable models with requirements beyond standard model physics with very large couplings [29, 30]. Localized energy injection around matter-radiation equality has also been invoked to reduce the sound horizon and increase the Hubble constant by introducing early dark energy [31, 32]. However, these models suffer fine tuning problems at eV scales and also lead to severe scale dependent changes in the matter spectrum, which worsen the  $\sigma_8$  tension

[33]. They also shift some standard  $\Lambda$ CDM parameters [34], in particular the spectral index  $n_s$  and the physical baryon density  $\Omega_b h^2$  ( $h = H_0/100$  km/s/Mpc).

On the other hand, proposals to reduce the  $H_0$  tension through modifications of late universe physics have included interacting dark matter [35], emergent dark energy [36] and modified gravity [37]. Furthermore, a closed universe scenario was also suggested to solve some internal inconsistencies between high- $\ell > 800$  and low- $\ell < 800$  observations in the Planck data [38]. However, it has been shown that when BAO is combined with Planck all parameters are enforced to flat  $\Lambda$ CDM even by considering the extension to 12 parameter space, which suggests even fundamentally radical extensions to the standard model need to keep the basic phenomenological elements of its success [39].

Here we test an alternative to  $\Lambda$ CDM through a particular modification of gravity, which leaves the early universe compatible with the CMB as measured by Planck. This is accomplished in terms of infrared (IR) gravity corrections within the  $f(T)$  teleparallel gravity. As is well known, this type of modification acts effectively as a phantom DE without breaking the null energy condition [40–42]. It can also completely resolve the  $H_0$  tension between the CMB and local measurements, even if tension remains with BAO measurements [43]. A major detriment of such modified gravity models however is that they normally introduces extra free parameters to the usual six parameters of the  $\Lambda$ CDM (see [44]).

In the present study We examine the cosmological viability of a model that does not introduce any such parameters. This is the exponential IR teleparallel gravity:  $f(T) = T e^{\beta T_0/T}$ , where  $T$  is the teleparallel torsion scalar and  $\beta$  is a dimensionless parameter. The theory has been previously introduced to provide a viable dynamical phase portrait compatible with the late transition from decelerated to accelerated expansion [45]. In the present paper (hereafter paper I), we confront this theory with various data sets, in order to test its empirical viability at the background expansion history, including the effect of modified background expansion on the growth of linear matter perturbation. The full linear perturbation analysis of the theory, with the full CMB powerspectra using Planck 2018 legacy, will be given elsewhere [46] (hereafter paper II).

In Sec. 2, we review the  $f(T)$  teleparallel gravity and its effect on the cosmological background evolution and dark matter growth rate. In Sec. 3, we discuss the particular  $f(T)$  theory studied here. In Sec. 4, we list and discuss the observational constraints we consider in order to examine the empirical viability of the proposed  $f(T)$  theory, and perform the joint likelihood analysis to obtain the best-fit values of the free parameters for both  $\Lambda$ CDM and  $f(T)$ -CDM models. In Sec. 5, we discuss the viability of the  $f(T)$  gravity according to the obtained results. In Sec. 6 we summarise our results and discuss prospects for future work.

## 2 $f(T)$ cosmology

Consider a 4-dimensional  $C^\infty$ -manifold  $(\mathcal{M}, e_a)$ , where  $e_a$  are four linear independent vector (tetrad, vierbein) fields defined on  $\mathcal{M}$ . The vierbein fields fulfil the conditions  $e_a^\mu e^a_\nu = \delta_\nu^\mu$  and  $e_a^\mu e^b_\mu = \delta_a^b$ , where the summation convention is assumed for both Latin (tangent

4-spacetime coordinates), and Greek (4-spacetime coordinates) [47, 48]. The spacetime metric is related to the vierbein by

$$g_{\mu\nu} \equiv \eta_{ab} e^a{}_\mu e^b{}_\nu, \quad (2.1)$$

where  $\eta_{ab}$  is the tangent space Minkowski metric. Moreover, one can straightforwardly construct the teleparallel geometry by finding the nonsymmetric (Weitzenböck) linear connection  $\Gamma^\beta{}_{\mu\nu} \equiv e_a{}^\beta \partial_\nu e^a{}_\mu = -e^a{}_\mu \partial_\nu e_a{}^\beta$ . Since  $\Gamma^\beta{}_{\mu\nu}$  is nonsymmetric, it defines the torsion tensor

$$T^\beta{}_{\mu\nu} \equiv \Gamma^\beta{}_{\nu\mu} - \Gamma^\beta{}_{\mu\nu} = e_a{}^\beta (\partial_\mu e^a{}_\nu - \partial_\nu e^a{}_\mu), \quad (2.2)$$

while its curvature vanishes identically. Thus, in this approach, gravity is encoded in terms of torsion instead of curvature, as in GR. In teleparallel geometry, one can define the teleparallel torsion scalar,

$$T = \frac{1}{4} T^\alpha{}_{\mu\nu} T^{\mu\nu}{}_\alpha + \frac{1}{2} T^\alpha{}_{\mu\nu} T^{\mu\nu}{}_\alpha - T^\alpha{}_{\mu\alpha} T^{\alpha\mu}{}_\alpha, \quad (2.3)$$

which is equivalent to the Ricci scalar  $R$  up to a total derivative term. It therefore generates the same set of field equations as GR when it replaces  $R$  in Einstein-Hilbert action. However the extension to  $f(T)$  theories differs from  $f(R)$  in its structure and consequences (see the review [49] for details). The most crucial difference is that the  $f(T)$  field equations are not invariant under local Lorentz transformation in its pure tetrad (trivial spin connection) formalism [50, 51]. However, a fully covariant version of the theory has been obtained by considering the spin connection contribution to the field equations [52]. The misconception regarding their local Lorentz invariance in the  $f(T)$  gravity has been also discussed in details in [48]. In addition, it has been shown that the gravitational waves, within  $f(T)$  gravity, propagate with exactly the speed of light, which makes the theory compatible with the observation of GW170817 and its electromagnetic counterpart GRB170817A [53], see also [54]. To evaluate the gravitational field produced by  $f(T)$  gravity, we write the action

$$\mathcal{S} = \frac{1}{2\kappa^2} \int d^4x |e| f(T) + \mathcal{S}_M, \quad (2.4)$$

where  $|e| = \sqrt{-g} = \det(e_\mu{}^a)$ , the constant  $\kappa$  is related to the Newton's constant  $G_N$  via  $\kappa^2 = 8\pi G_N$  and  $\mathcal{S}_M$  is the action of the matter fields. The variation with respect to the vierbein gives rise to the field equations

$$\frac{1}{\kappa_{eff}^2} \mathfrak{G}_{\mu\nu} = \mathfrak{T}_{\mu\nu}^M + \mathfrak{T}_{\mu\nu}^{DE}, \quad (2.5)$$

where  $\kappa_{eff}^2 = \kappa^2/f_T$ , and we take the perfect fluid approximation to describe the matter content

$$\mathfrak{T}_{\mu\nu}^M = \rho u_\mu u_\nu + p (u_\mu u_\nu + g_{\mu\nu}), \quad (2.6)$$

where  $\rho$ ,  $p$  and  $u^\mu$  are the density, pressure and 4-velocity unit vector of the fluid, respectively. This defines the “geometrical” DE component via

$$\mathfrak{T}_{\mu\nu}^{DE} = \frac{1}{\kappa^2} \left( \frac{1}{2} g_{\mu\nu} (T f_T - f) - f_{TT} S_{\nu\mu\rho} \nabla^\rho T \right). \quad (2.7)$$

We assume the background geometry of the universe to be flat Friedmann-Lemaître-Robertson-Walker (FLRW). Hence, we take the Cartesian coordinate system  $(t; x, y, z)$  and the diagonal vierbein

$$e_\mu^a = \text{diag}(1, a(t), a(t), a(t)), \quad (2.8)$$

where  $a(t)$  is the scale factor of the universe. One can show that the above vierbein, via Eq. (2.1), generates the flat FLRW spacetime metric

$$ds^2 = dt^2 - a(t)^2 \delta_{ij} dx^i dx^j, \quad (2.9)$$

where the Minkowskian signature is  $\eta_{ab} = (+, -, -, -)$ . We note that this choice of the vierbein in Eq. (2.8) is already in the proper form, since the associated spin connection is flat and subsequently leads to symmetric field equations for any  $f(T)$  theory [48] (see also [49, 52, 55, 56]). The diagonal vierbein Eq. (2.8) directly relates the teleparallel torsion scalar (Eq. (2.3)) to Hubble rate as follows:

$$T = -6H^2, \quad (2.10)$$

where  $H \equiv \dot{a}/a$  is Hubble parameter, and the ‘‘dot’’ denotes differentiation with respect to the cosmic time  $t$ .

## 2.1 $f(T)$ modification of the background dynamics

The field equations corresponding to the vierbein in Eq. (2.8) give rise, respectively, to the Friedmann and Raychaudhuri equations

$$\frac{3}{\kappa^2} H^2 = \rho_m + \rho_r + \rho_T \equiv \rho_{eff}, \quad (2.11)$$

$$-\frac{1}{\kappa^2} (3H^2 + 2\dot{H}) = p_r + p_T \equiv p_{eff}. \quad (2.12)$$

The torsion density and pressure, using (2.10), in the above equations are given by

$$\rho_T = \frac{1}{2\kappa^2} (6H^2 - f + Hf_H), \quad (2.13)$$

$$p_T = -\frac{1}{6\kappa^2} \dot{H}(12 + f_{HH}) - \rho_T, \quad (2.14)$$

where  $f = f(H)$ ,  $f_H = \frac{df}{dH}$  and  $f_{HH} = \frac{d^2f}{dH^2}$ .

Also, we write the continuity equations of the pressureless matter (baryon + cold dark matter), radiation and the torsion (respectively)

$$\dot{\rho}_m + 3H\rho_m = 0, \quad (2.15)$$

$$\dot{\rho}_r + 4H\rho_r = 0, \quad (2.16)$$

$$\dot{\rho}_T + 3(1 + w_T)H\rho_T = 0, \quad (2.17)$$

where the torsion equation of state  $w_T$  is given by

$$w_T = \frac{p_T}{\rho_T} = -1 + \frac{(f_{HH} + 12)(f - Hf_H)}{f_{HH}(f - 6H^2 - Hf_H)}. \quad (2.18)$$

It is useful to define the effective (total) equation-of-state parameter

$$w_{eff} \equiv \frac{p_{eff}}{\rho_{eff}} = -1 - \frac{2}{3} \frac{\dot{H}}{H^2}, \quad (2.19)$$

which can be related to the deceleration parameter  $q$  by the following expression

$$q \equiv -1 - \frac{\dot{H}}{H^2} = \frac{1}{2} (1 + 3w_{eff}). \quad (2.20)$$

A nice feature of the  $f(T)$  field equations is that they are of second order, unlike other gravitational theories; e.g.,  $f(R)$  field equations, which are fourth order. Furthermore, this family of governing equation of any  $f(T)$  theory reduces to a one-dimensional autonomous system, similar to GR. This makes the  $f(T)$  gravity a natural generalization of GR, whereas the governing equation is given by [45]

$$\dot{H} = 3(1+w) \frac{f - Hf_H}{f_{HH}} = \mathcal{F}(H). \quad (2.21)$$

This dynamical view enables the succinct visualization of the global dynamics of the system through the corresponding phase portrait in the  $H, \dot{H}$  phase-space.

## 2.2 $f(T)$ modification of growth function

In the framework of  $f(T)$  modified gravity, at Newtonian sub-horizon scales, one can expect that the dark energy is smooth and consider linear perturbations only on the matter sector, whereas changes in the evolution of the growth of structure is determined by modified background expansion effects on the growth rate. In particular, the Hubble expansion rate  $H$  and the effective Newton's gravitational constant  $\kappa_{eff}^2 = \kappa^2/f_T$ ; c.f. [44, 57, 58] and discussion below.

It is convenient to work in the Newtonian gauge for perturbations around the metric (2.9), i.e

$$ds^2 = (1 + 2\Psi)dt^2 - a^2(t)(1 - 2\Phi)\delta_{ij}dx^i dx^j, \quad (2.22)$$

which is a well-defined gauge without any residual gauge freedom, and with two scalar gravitational potentials  $\Psi$  and  $\Phi$  for describing deviations from the background metric. These are crucial for large-scale structure and weak lensing studies, in addition to the matter density contrast<sup>1</sup>  $\delta_m = \delta\rho_m/\rho_m$ . In effect, the gauge invariant comoving density contrast is given by

$$\Delta_m = \delta_m + \frac{3aH}{k} \theta_m, \quad (2.23)$$

where  $k$  is the wave number in Fourier space and  $\theta_m$  is the divergence of the fluid velocity.

In the conformal Newtonian gauge, and in Fourier space, a generic departure from GR scenario of scalar perturbation growth can be represented by introducing two parameters  $Q(a, k)$  and  $\eta(a, k)$  [59], whereas

$$k^2 \Phi = \frac{1}{2} \kappa^2 Q(a, k) a^2 \rho_m \delta_m, \quad (2.24)$$

$$\Phi = \eta(a, k) \Psi. \quad (2.25)$$

---

<sup>1</sup>Here we focus on beyond radiation era dynamics.

In modified gravity,  $Q(a, k)$  represents a mass screening effect due to local modifications of gravity. It effectively modifies Newton's gravitational constant. On the other hand,  $\eta(a, k)$  represents the effective anisotropic stress introduced by modified gravity. In general, these two parameters have time and scale dependence. A generic modification of the dynamics of the linear matter perturbation can be represented via the matter continuity [59]

$$\Delta_m'' + \left(2 + \frac{H'}{H}\right)\Delta_m' - \frac{3}{2}\Omega_m(a)\frac{Q(a, k)}{\eta(a, k)}\Delta_m = 0, \quad (2.26)$$

where prime denotes the derivative  $d/d \ln a$  and  $\Omega_m(a) = (8\pi G_N/3H^2)\rho_m$ . In  $f(T)$  gravity, in particular on the sub-Hubble scale, the parameters  $Q(a, k) \rightarrow Q(a) = 1/f_T$  and  $\eta(a, k) \rightarrow 1$ , whereas GR, i.e  $f(T) = T$ , is recovered as a particular case.

In the present context, the evolution of the comoving density contrast  $\Delta_m$  in  $f(T)$  is scale independent as in GR but driven by the product  $\Omega_m(a)Q(a) = \Omega_m(a)/f_T$ . Therefore, in this context,  $f(T)$  gravity modifies the growth of structure in a way very similar to the GR theory, this is in contrast to  $f(R)$  gravity which includes scale dependence effects. The formulation here however is valid solely at sub-horizon scale  $k \gg aH$ , otherwise the equation for growth has a complicated form [57, 60], which may lead to a large deviation from  $\Lambda$ CDM in the matter power spectra. This will be revisited in paper II [46], when the full perturbation analysis is adopted.

As linear matter perturbations in the Newtonian limit are sensitive to the background modifications through  $H(a)$  and the effective Newton's constant  $\kappa^2/f_T$ , one can include growth rate observations in the viability test of the exponential IR  $f(T)$  gravity at the background level. We define the growth factor of the matter density contrast

$$G = \frac{\Delta_m(a, k)}{\Delta_{m,0}(1, k)}, \quad (2.27)$$

where  $\Delta_{m,0}(1, k)$  is the comoving density contrast current value. In practice, one considers the product  $f\sigma_8$  to test the viability of the model with the red-shift space distortion observations, where the cosmological growth rate is given by

$$f = \frac{d \ln G}{d \ln a}, \quad (2.28)$$

and  $\sigma_8$  is the standard deviation of the overdensity  $\delta_m$  measured in spheres of radius  $8 h^{-1} Mpc$ . By solving Eq. (2.26) with (2.27) and (2.28), one can confront the theory with the RSD observations (see Sec. 5.4).

### 3 The exponential IR $f(T)$ model

Several  $f(T)$  theories have been proposed in the literature with the aim of realizing late accelerated expansion. Such theories are generally characterized by one or two model parameters [61–63]. Under particular choices of the parameters, models that have been hitherto shown viable essentially reduce to  $\Lambda$ CDM cosmology but include an extra parameter relative to that standard model, which makes the latter preferable given similar fits to the data.

Motivated by the phase portrait patterns of viable models, a new  $f(T)$  theory has been proposed to produce late acceleration expansion [45]

$$f(T) = T e^{\beta(T_0/T)}, \quad (3.1)$$

where  $T_0 = -6H_0^2$  and  $\beta$  is a dimensionless parameter. Following [44], the modified Friedmann equation can be rewritten as

$$E^2(z) = \Omega_m(1+z)^3 + \Omega_r(1+z)^4 + \Omega_T y(z). \quad (3.2)$$

Here  $E(z) = H(z)/H_0$ ,  $\Omega_i$  is current value of density parameter (the subscript  $i$  denotes  $m$ ,  $r$  and  $T$  for matter, radiation and torsion),  $\Omega_T = 1 - \Omega_m - \Omega_r$ , and the distortion function  $y(z)$  is given by

$$y(z) = \frac{6H^2 - f(H) + Hf_H}{6\Omega_T H_0^2}, \quad (3.3)$$

where we adopted  $T-H$  relation, namely Eq. (2.10). From Eq. (3.1), the distortion function becomes

$$y(z) = \Omega_T^{-1} \left( E^2 - (E^2 - 2\beta)e^{\frac{\beta}{E^2}} \right), \quad (3.4)$$

and consequently the Friedmann equation (Eq. (3.2)) reads

$$(E^2 - 2\beta)e^{\frac{\beta}{E^2}} = \Omega_m(1+z)^3 + \Omega_r(1+z)^4. \quad (3.5)$$

At the present epoch, i.e  $z = 0$  and  $E = 1$ , the  $\beta$ -parameter can be expressed in terms of the current values of the density parameters as

$$\beta = \frac{1}{2} + \mathcal{W} \left( \frac{\Omega_m + \Omega_r}{-2e^{\frac{1}{2}}} \right), \quad (3.6)$$

where  $\mathcal{W}(x)$  is the Lambert  $\mathcal{W}$  function<sup>2</sup>. At present, the radiation density parameter  $\Omega_r = \Omega_\gamma \left[ 1 + \frac{7}{8} \left( \frac{4}{11} \right)^{4/3} N_{eff} \right]$ , whereas the photon density parameter  $\Omega_\gamma = 2.4728 \times 10^{-5} h^{-2}$ , and the effective number of neutrino species as in standard model  $N_{eff} = 3.046$ . Thus the advantage of this model is that it does not introduce any new parameters in the Friedmann equation (Eq. (3.5)), other than those in  $\Lambda$ CDM, i.e  $\{\Omega_m, H_0\}$ . The preliminary analysis of the theory shows that it can pass the basic requirements to be considered in literature [45]. In the present work, we confront this model with various cosmological observations which put precise constraints on the model.

The GR limit of the modified Friedmann equation ((3.5)) is recovered by setting  $\beta = 0$ . The theory does not produce  $\Lambda$ CDM for any value of  $\beta$ . For larger Hubble values, the model reduces to GR. On the contrary, in the small Hubble regime we expect deviations from the GR limit on the large scales, notably giving rise to accelerated expansion that does not necessarily correspond to that induced by a cosmological constant. Remarkably, at redshift  $z \rightarrow -1$ , we get  $E^2 \rightarrow 2\beta$ . This is in fact a future de Sitter fixed point but pushed up to  $t \rightarrow \infty$ .

---

<sup>2</sup>Defined via  $x = \mathcal{W}(x) \exp \mathcal{W}(x)$ .

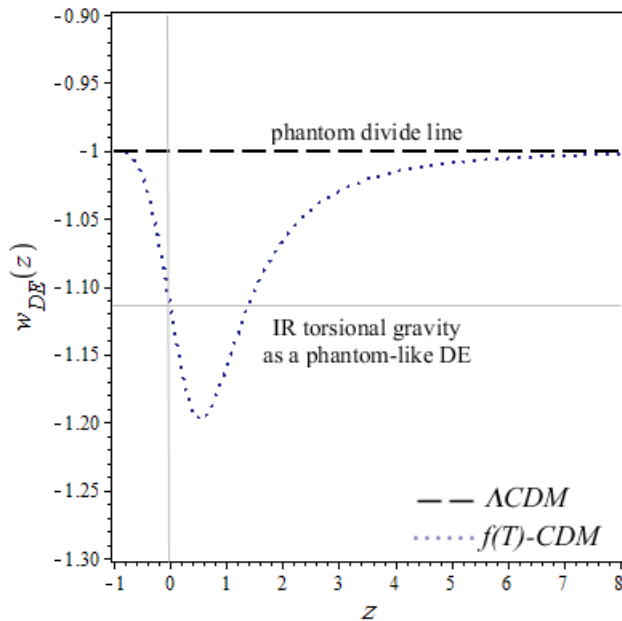


**Figure 1.** The evolution of torsional gravity counterpart. It illustrates the effective dark energy role and phantom-like nature of the IR gravity corrections.

Recalling Eq. (2.18), one finds that the torsional gravity counterpart,  $w_T$ , evolves as a phantom-like DE, as probed in Fig. 1. As is well known, the infrared (IR) correction of gravity produces an apparent phantom dark energy  $w < -1$  without violating the null energy condition [41, 42]. In its context the late accelerated expansion is realized by weakening the general relativistic gravity at the IR scales (cosmic distances), while keeping its successes at smaller scales. As already mentioned, the detailed scale dependence of this weakening is discussed through perturbation analysis in [46].

In Fig. 1 we show the general behavior of torsion acting as DE. At large  $z$ , we have  $w_T(z) \rightarrow -1$ , as with a cosmological constant. Nevertheless,  $\rho_T = -p_T \rightarrow 0^+$ , unlike a cosmological constant, which has fixed density and pressure at all time. At low redshifts  $z \sim 8$ , the torsional counterpart evolves as phantom DE. At present  $w_T \approx -1.12$ , while it is evolving towards pure de Sitter spacetime with  $w_T \rightarrow -1$  as  $z \rightarrow -1$  (i.e  $t \rightarrow \infty$ ).

#### 4 Observational constraints and datasets

We employ different datasets to constrain the exponential IR  $f(T)$  gravity, testing its viability as a model of late-time cosmic acceleration. The same analysis is applied to  $\Lambda$ CDM for comparison. In the following subsections we give a brief description of those different datasets and the methodology used in the present analysis.

## 4.1 Astronomical datasets

### 4.1.1 Supernovae type Ia

Type Ia supernovae as standard candles have been crucial to cosmology since leading to the discovery of cosmic acceleration in the late 1990’s [64, 65]. In comparison with BAO and CMB data, SNIa data is however statistically less potent in constraining  $\Lambda$ CDM model in general. They remain nevertheless essential for testing background cosmological evolution models at low redshifts, which is the main concern of our present analysis.

The SNIa distance modulus  $\mu$  is related to the luminosity distance  $D_L$  via the relation

$$\mu(z) \equiv m(z) - M = 5 \log_{10}(D_L) + 25, \quad (4.1)$$

where  $m$  is the apparent magnitude and  $M$  is the absolute magnitude. The distance  $D_L$ , in Mpc, is given by

$$D_L = \frac{(1+z)}{H_0} \int_0^z \frac{dz'}{E(z')}, \quad (4.2)$$

for a flat FLRW model (i.e.  $\Omega_K = 0$ ). As in Eq. (4.2), the luminosity distance is solely determined by the modified Friedman equation, Eq. (3.5). To get the background dynamics of the  $f(T)$ -CDM model, we numerically solve Eq. (3.5) by means of iterative method. Pantheon SNIa observed distance modulae are calculated using the B-Band apparent and absolute magnitudes. The absolute magnitude  $M$  is almost constant for all supernovae and is taken as an inference parameter.

We use the ‘‘Pantheon’’ sample from [66], with 276 additional supernovae to the ‘‘Joint Light-curve Analysis’’ (JLA) sample [67–69] from the Pan-STARRS1 Medium Deep Survey plus low-redshift and Hubble space telescope (HST) samples with a total of 1048 supernovae spanning redshift range  $0.01 < z < 2.3$ . Note that from Eqs. (4.1) and (4.2), the SNIa distance modulus only constrains parameters in the function  $E(z)$ . This is known as distance-redshift degeneracy [70]; the absolute magnitude  $M$  is degenerate with the Hubble constant  $H_0$ .

### 4.1.2 $H_0$ measurements

Since SNIa data alone does not fix  $H_0$ , we take as a prior value of the Hubble constant, the distance-ladder estimate of  $H_0 = 73.52 \pm 1.62$  km/s/Mpc (hereafter R18) from the widely used SHOES project using Gaia parallaxes [9].

### 4.1.3 Baryon acoustic oscillation

We consider BAO radial measurements of  $H(z)r_{drag}$  along the line of sight, as well as the BAO transverse measurements of  $D_V(z)/r_{drag}$  perpendicular to the line of sight. Here  $r_{drag}$  is the comoving sound horizon at the end of the baryon drag, and  $D_V$  can be given as a combination of the comoving angular distance  $D_M(z) = D_L/(1+z)$  and the Hubble parameter  $H(z)$  given by

$$D_V(z) = \left[ D_M^2(z) \frac{cz}{H(z)} \right]^{\frac{1}{3}}. \quad (4.3)$$

We use the high precision measurements of the latest BOSS data release 12 (BOSS DR12) [71], which summarized "consensus" results on BAOs (first reported in [72, 73] and [74]) at effective redshift bins  $z_{eff} = 0.38, 0.51$  and  $0.61$ . In addition, we consider the two measurements of  $D_V/r_{drag}$  at low redshifts  $z_{eff} = 0.106$  and  $z_{eff} = 0.15$  by the 6dFGS [75] and SDSS-MGS [76], respectively. Moreover, we use the WiggleZ redshift survey reconstructed measurements [77], as well as the recent BAO measurement by eBOSS DR16, using multi-tracers in configuration space, at  $z = 0.77$  for  $D_H \equiv c/H(z) = 19.65 \pm 0.54 \times r_{drag}$  and  $D_M/r_{drag} = 18.93 \pm 0.37$  [78]. We note that, at low redshift, the combined BAO likelihood is dominated by the high precision measurements of BOSS DR12.

#### 4.1.4 Redshift-space distortion

Peculiar motions of galaxies introduce anisotropies in the galaxy clustering observed in redshift surveys. This phenomenon is known as Redshift-Space Distortions (RSD). The measurements of RSD could constraint the amplitude of the matter power spectrum, and in turn the structure growth rate [79]. Usually measurements of RSD are given in terms of  $f\sigma_8$ , where the growth rate  $f$  is as given via (2.28). For  $\Lambda$ CDM, the growth rate is approximated by the parametrization  $f \sim \Omega_m^{0.55}(z)$ . For the  $f(T)$ -CDM model, we numerically solve Eq. (2.26) for the growth function  $\Delta_m$ .

We use RSD measurements of  $f\sigma_8$  from BOSS DR12 results [72], together with WiggleZ [80], eBOSS DR16 [78], SDSS MGS [81], 6dFGRS [82], and the growth rate constraint by [83] (obtained by comparing observed Fundamental Plane peculiar velocities in 6dFGS with predicted velocities and densities from the 2M++ redshift survey).

## 4.2 Cosmological constraints and allowed parameter space

### 4.2.1 BBN constraint on Baryon density

We use the conservative prior on the baryon density  $\omega_b = \Omega_b h^2 = 0.0222 \pm 0.0005$  (68% CL), as calculated by Planck 2018 [5], and found to be compatible with the three BBN calculation pipelines based on the deuterium abundance measurement [84].

### 4.2.2 CMB constraints

We add a conservative CMB "BAO" measurement of the angular acoustic scale at decoupling  $\theta_s = \theta(z_s)$ , where  $z_s$  defines the redshift at which the optical depth equals unity; i.e.,  $\tau(z_s) = 1$ . We use the constraints on the base parameters obtained from Planck 18 (TT,TE,EE+lowE+lensing) dataset [5], to obtain the value of  $100\theta_s = 1.04190 \pm 0.00030$  using the CLASS code. Since this parameter is measured with a precision of sub-percent level, the procedure allows for a tight constraint on the parameter space, comparable to those obtained from the full CMB dataset.

We note that the value derived for  $\theta_s$  using the CLASS code (in the current analysis) agrees with the  $\theta_{MC}$  presented in Planck results (which is derived using CAMB and CosmoMC codes) within  $1\sigma$ . It is also worth mentioning that  $\theta_s$  is the actual angular scale of the sound horizon at decoupling, obtained by fully integrating over the sound speed and then searching numerically for the time of decoupling (defined as the maximum of the visibility

function). On the other hand,  $\theta_{\text{MC}}$  is an approximation based on a model-dependent analytical fits instead of the full integral [85].

Finally, we fix two parameters as measured by CMB Planck 2018 [5], namely the optical depth at reionization  $\tau(z_{re}) = 0.0544 \pm 0.0073$  and the spectral index  $n_s = 0.9649 \pm 0.0042$ .

### 4.2.3 Parameter space

For both the  $\Lambda$ CDM and  $f(T)$ -CDM models, we take the Base dataset as SNIa +  $H_0$  + BBN + BAO, which allows to fix three parameters  $\{H_0, \Omega_b, \Omega_c\}$ . By adding the RSD data, we can fix one more parameter, that is the amplitude of the growth of structure  $\{\sigma_8\}$ . In addition, the inclusion of the CMB  $\theta_s$  allows for better constraints on the full parameter space

$$\mathcal{P} = \{H_0, \Omega_b, \Omega_c; \sigma_8\}. \quad (4.4)$$

We also give some additional derived parameters, namely  $\{\Omega_m, \theta_s, r_{\text{drag}}, z_{re}, S_8\}$ , where  $\Omega_m = \Omega_b + \Omega_c$ ,  $\theta_s$  the angular size of the sound horizon at recombination,  $z_{re}$  is the reionization redshift and  $S_8 = \sigma_8 \sqrt{\Omega_m/0.3}$ ; in addition to the absolute magnitude,  $M$ , as an inference parameter.

We use the CLASS code [85], together with Monte Python [86], after proper modifications (for the computation of  $f(T)$ -CDM background dynamics) to run Monte Carlo Markov Chain (MCMC) analysis. In order to analyze the resulting MCMC chains and obtain the contour plots of the different model parameters, we use of GetDist python package [87].

## 5 Results

In this section we test the viability of the  $f(T)$ -CDM theory with a full likelihood analysis and compare it in relation to  $\Lambda$ CDM. We also examine the consistency of the obtained results in light of the different datasets listed and described above. We point out the recent tensions between different datasets and discuss prospects for resolution within the exponential IR  $f(T)$  theory.

### 5.1 Viability of the $f(T)$ -CDM model

As the current  $f(T)$  theory has the same number of free parameters as  $\Lambda$ CDM model, a direct statistical comparison using a  $\chi^2$  is straightforward.

In Table 1, we list the best-fit values up to 68% CL, for both  $\Lambda$ CDM and the exponential IR  $f(T)$  theory, using different combinations of cosmological datasets; such as Base ( $\equiv$  SNIa+ $H_0$ +BBN+BAO), Base+RSD and Base+RSD+CMB  $\theta_s$ . As can be seen, the minimum Chi-squares ( $\chi_{\text{min}}^2$ ) for both models are comparable, with slight preference of  $f(T)$  for all dataset combinations, which confirms the viability of the  $f(T)$ -CDM model. We note that by utilizing the concise CMB measurement of the angular scale of the sound horizon,  $\theta_s$ , we obtain more constrained values of the inferred parameters, while keeping the agreement of the two models within  $1\sigma$ .

In Fig. 2, we plot the 2D joint contours of the model parameters  $\{\Omega_c, \Omega_b, \sigma_8\}$  versus  $H_0$ , for  $\Lambda$ CDM and  $f(T)$ -CDM scenarios at 68% and 95% confidence level (CL). This was

**Table 1.** 68% parameter intervals for  $\Lambda$ CDM and  $f(T)$ -CDM models from SNIa,  $H_0$ , BAO, BBN, RSD and CMB  $\theta_s$  measurements grouped in these datasets. The minimum value of  $\chi^2$  for each model is given in the last row. Here “Base” represents SNIa,  $H_0$ , BBN and BAO joint dataset.

Parameter	$\Lambda$ CDM			$f(T)$ -CDM		
	Base	Base+RSD	Base+RSD+CMB $\theta_s$	Base	Base+RSD	Base+RSD+CMB $\theta_s$
	68% limits	68% limits	68% limits	68% limits	68% limits	68% limits
$H_0$ .....	$68.3^{+1.0}_{-1.3}$	$68.4 \pm 1.0$	$68.30 \pm 0.77$	$70.7 \pm 1.3$	$70.6^{+1.3}_{-1.2}$	$70.52 \pm 0.71$
$\Omega_b$ .....	$0.0477 \pm 0.0017$	$0.0477^{+0.0015}_{-0.0017}$	$0.0478 \pm 0.0011$	$0.0438^{+0.0014}_{-0.0017}$	$0.0440^{+0.0013}_{-0.0016}$	$0.04485 \pm 0.00090$
$\Omega_c$ .....	$0.256^{+0.017}_{-0.020}$	$0.255 \pm 0.017$	$0.2516 \pm 0.0086$	$0.272 \pm 0.018$	$0.270 \pm 0.018$	$0.2486 \pm 0.0072$
$\sigma_8$ .....	–	$0.782 \pm 0.024$	$0.781 \pm 0.025$	–	$0.766 \pm 0.033$	$0.781^{+0.035}_{-0.040}$
$\Omega_m$ .....	$0.305^{+0.016}_{-0.018}$	$0.304 \pm 0.016$	$0.3008 \pm 0.0092$	$0.317 \pm 0.017$	$0.315 \pm 0.017$	$0.2947 \pm 0.0077$
$100\theta_s$ .....	$1.044^{+0.014}_{-0.016}$	$1.044^{+0.015}_{-0.013}$	$1.04189^{+0.00030}_{-0.00033}$	$1.055^{+0.017}_{-0.015}$	$1.054^{+0.016}_{-0.014}$	$1.04192 \pm 0.00030$
$r_{drag}$ .....	$147.413^{+7.594}_{-7.626}$	$147.377^{+7.256}_{-7.387}$	$147.821^{+4.322}_{-4.981}$	$143.611^{+11.349}_{-8.026}$	$143.913^{+10.767}_{-7.88}$	$146.189^{+5.496}_{-4.385}$
$z_{re}$ .....	$7.51^{+0.22}_{-0.25}$	$7.49 \pm 0.23$	$7.46 \pm 0.13$	$7.84 \pm 0.24$	$7.81^{+0.26}_{-0.22}$	$7.53 \pm 0.12$
$S_8$ .....	–	$0.786 \pm 0.025$	$0.782 \pm 0.025$	–	$0.785 \pm 0.035$	$0.774^{+0.035}_{-0.041}$
$M$	$-19.401^{+0.038}_{-0.046}$	$-19.399 \pm 0.037$	$-19.402 \pm 0.021$	$-19.352 \pm 0.047$	$-19.355^{+0.047}_{-0.042}$	$-19.365 \pm 0.019$
$\chi^2_{min}$	519.411	523.893	525.862	516.441	518.091	524.465

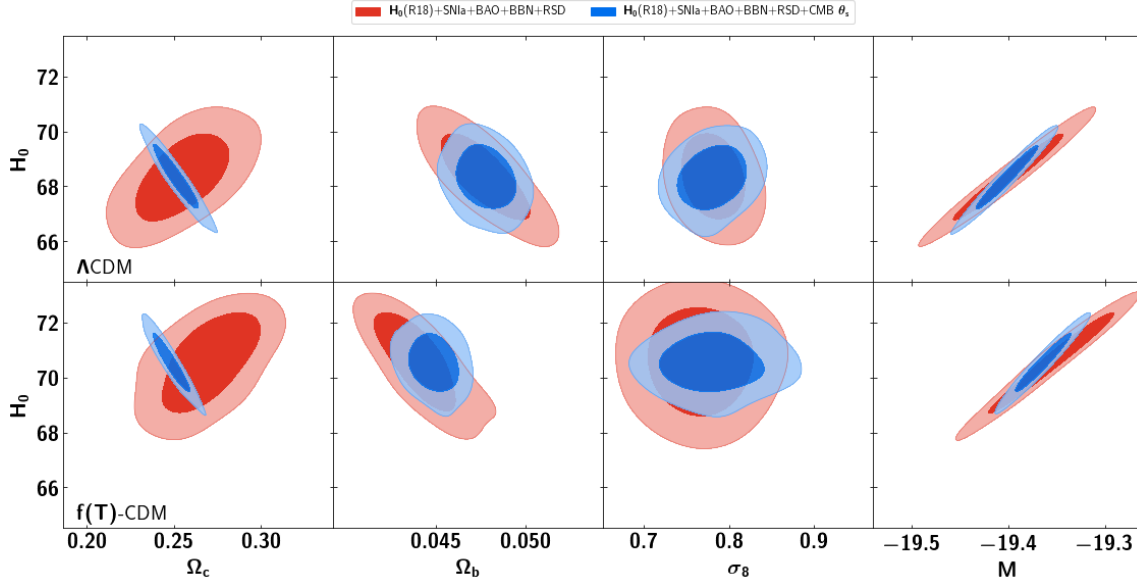


**Figure 2.** A compilation of  $1\sigma$  and  $2\sigma$  contour plots for the four parameters,  $\Omega_c$ ,  $\Omega_b$  and  $\sigma_8$ , on the horizontal axis, plus  $H_0$  on the vertical access, and the inference parameter  $M$  on the horizontal axis. This is shown for both  $\Lambda$ CDM, in the upper panel, and  $f(T)$ -CDM model, in the lower panel. Red contours represent the joint likelihood analysis for SNIa,  $H(z)$ , BAO, BBN and RSD datasets, while blue contours include in addition the BAO measurement of the CMB (namely the angular acoustic scale  $\theta_s$  measurement).

done using the full likelihood analysis for the full set of parameters, including the inferred ‘nuisance’ parameter  $M$ , for two main datasets (with/without CMB  $\theta_s$  constraint). As is apparent, with the inclusion of the Planck constraint on the CMB  $\theta_s$ , both  $\Lambda$ CDM and

$f(T)$ -CDM remain in agreement, while the latter gives higher  $H_0$  value compared to  $\Lambda$ CDM, indicating a partial solution of the associated tension.

## 5.2 Consistency with observations

We examine the consistency of the obtained results from the joint MCMC likelihood with individual observational datasets; namely how they fare separately with SNIa, BAO and RSD. We use the best fit values, in particular the full dataset combination Base+RSD+CMB  $\theta_s$ , as provided by Table 1 for both the  $\Lambda$ CDM and the exponential IR  $f(T)$  models.

In the upper panel of Fig. 3, Pantheon data are compared with  $\Lambda$ CDM and  $f(T)$ -CDM models with best-fit parameters values. Both are in a good agreement with SNIa data. We note that the  $\Lambda$ CDM and  $f(T)$ -CDM models give, respectively, absolute magnitudes  $M = -19.402 \pm 0.021$  and  $M = -19.365 \pm 0.019$  which are close to the true absolute magnitude of SNIa,  $M = -19$ .

In the second panel of Fig. 3, we show how well  $\Lambda$ CDM model fits  $H(z)$  BAO measurements, as provided by the precise constraints of BOSS DR12 and the recent eBOSS DR16 observations over redshift range  $0.3 < z < 1$ . However, it fails to reach local measurement of  $H_0$  value at  $z = 0.0$  [9]. On the other hand,  $f(T)$ -CDM tends to reach higher  $H_0$  value in better agreement with the local  $H_0$  measurement while keeping the good fit with the BAO  $H(z)$  measurements.

In the third panel of Fig. 3, we plot various BAO data used in this analysis in comparison with the theoretical prediction from  $f(T)$ -CDM model. We show the distance of the acoustic-scale ratio  $D_V/r_{drag}$  at several effective redshifts (as given in the figure), divided by the acoustic-scale ratio in the  $\Lambda$ CDM model. Both  $\Lambda$ CDM and  $f(T)$ -CDM (with best fit parameters) seem to agree very well with BAO measurements. We note that the exponential IR  $f(T)$  gravity entails a relatively mild phantom regime later in cosmic expansion history relative to the power law models discussed in [43]. Additionally, the current treatment only partially alleviates the  $H_0$  tension. In this context, the stark inconsistencies with BAO distances found in the aforementioned work are avoided.

In the bottom panel of Fig. 3, we use the best fit values of Table 1 to plot the theoretical predictions of the rate of the growth of structure diagnostic  $f\sigma_8$  for  $\Lambda$ CDM and  $f(T)$ -CDM models. Both models seem to agree perfectly with the RSD dataset.

Another consistency test of the exponential IR  $f(T)$  gravity is the age of the universe as predicted by the theory. According to the full likelihood results, as given in Table 1, the age of the universe is  $\sim 13.76$  Gyr, which is not in conflict with any of the known astrophysical observations so far [88–90].

We conclude that the exponential IR  $f(T)$  theory is statistically similar to  $\Lambda$ CDM, since both have the same number of free parameters. The  $\chi^2$  results are almost the same as for  $\Lambda$ CDM for the different dataset combinations in Table 1. The  $f(T)$  theory however shows some deviations at low redshifts as clear from Fig. 3 with  $H(z = 0)$  and  $f\sigma_8$ . We focus on the tensions related to these quantities in the following.

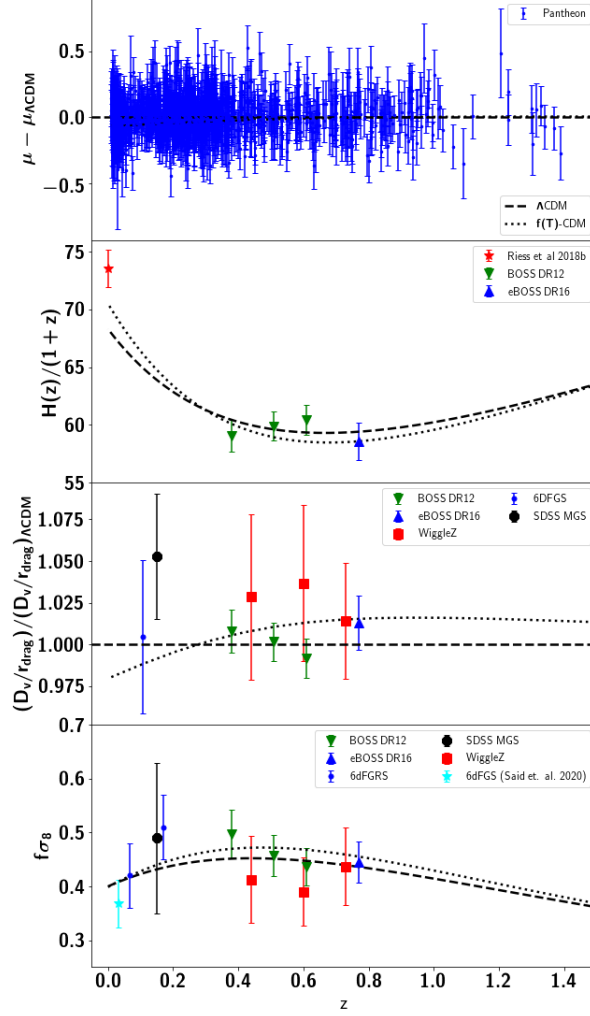


**Figure 3.** Various datasets are compared with theoretical predictions of  $\Lambda$ CDM and  $f(T)$ -CDM models, as given in Table 1. Upper panel: Residual of SNIa distance modulus measurements (blue dots) of Pantheon data sample from  $\Lambda$ CDM model. Second panel: Measurements of the Hubble parameter  $H$  from R18 local measurement (red star), BOSS DR12 BAO radial distance measurements (green down triangles) and eBOSS DR12 (blue up triangle). Third panel: the ratio of  $D_V$  over the comoving sound horizon at the baryon drag  $r_{drag}$  with respect to  $\Lambda$ CDM model from BOSS DR12 (green down triangles), WiggleZ (red squares), eBOSS DR12 (blue up triangle), low redshift 6DFGS (blue dot) and SDSS MGS (black pentagon) measurements. Bottom panel:  $f\sigma_8$  measurements from the same dataset as in the third panel in addition to 6dFGRS (blue dots) and the recent 6dFGS measurement (cyan star) [83].

### 5.3 The Hubble constant

As is clear from Table 1, the best fit values in parameter space for  $\Lambda$ CDM and the  $f(T)$ -CDM model are recognizably different when the CMB  $\theta_s$  is absent from the joint MCMC analysis (namely the Base and the Base+RSD combined data). However, the inclusion of the CMB

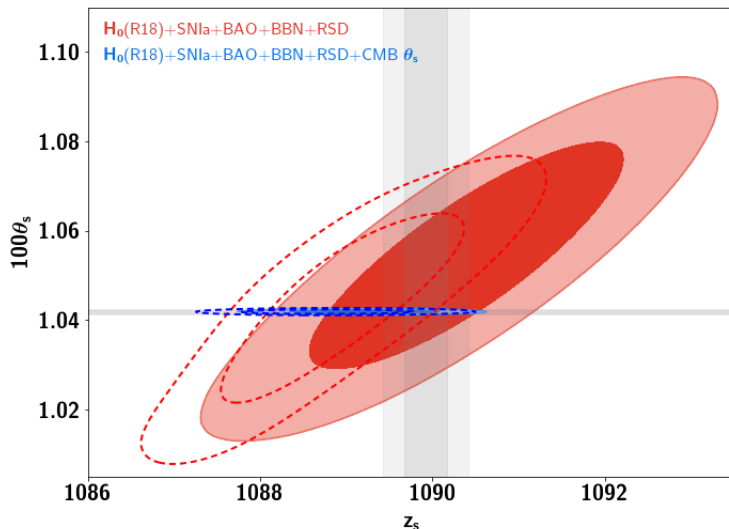


**Figure 4.** Constraints on  $100\theta_s-z_s$ : Solid contours are for  $f(T)$ -CDM and dashed contours are for  $\Lambda$ CDM model; grey bands represent  $1\sigma$  and  $2\sigma$  constraints from CMB Planck 2018 on the acoustic scale and the redshift at recombination [5]. In absence of any constraint from early universe on the CMB  $\theta_s$ , i.e the red contours, the  $f(T)$ -CDM theory predicts an acoustic scale a little bit different from  $\Lambda$ CDM predictions. This deviation can be understood in terms of slight different evolutions at late time, as clear in Fig. 3. However, by including an early universe constraint on the CMB  $\theta_s$ , i.e the blue contours, both models predict similar acoustic scales, in agreement with its Planck measurements within  $\sim 1\sigma$ , which shows that both models give same behaviors at recombination.

$\theta_s$  results in consistent values for the two models. This is understandable, as the angular acoustic scale is observationally pinpointed with  $\sim 0.03\%$  precision.

In order to illustrate how  $\Lambda$ CDM and  $f(T)$ -CDM fit with the Planck CMB measurements, we plot the  $\theta_s-z_s$  2D joint contours for both models. As can be seen from Fig. 4, the models provide slightly different values of  $\theta_s$  at recombination in absence of the CMB  $\theta_s$ , with a slight preference of  $f(T)$  gravity with Planck constraints. On the other hand, both fit well with Planck constraints at the recombination epoch, introduced by including the Planck constraint on the CMB  $\theta_s$ . This confirms that both models have similar early history.

Using the full likelihood, for  $\Lambda$ CDM we obtain  $H_0 = 68.30 \pm 0.77$  km/s/Mpc, which is  $2.9\sigma$  lower than the R18 local measurement of  $H_0$  [9]. On the other hand, for  $f(T)$ -CDM we obtain  $H_0 = 70.52 \pm 0.71$  km/s/Mpc, which is  $1.7\sigma$  lower than the local measurement; i.e. the  $f(T)$ -CDM is closer to the R18 measurement than  $\Lambda$ CDM by  $1.2\sigma$ . This, while keeping similar  $\chi^2_{min}$  for the full dataset. Thus, the analysis shows the Planck constraint on the CMB  $\theta_s$  fixes the early history of the two models similarly but allows the exponential IR  $f(T)$  theory to better fit with local  $H_0$  measurements.

In order to understand how these models take different tracks in the late universe, it is convenient to compare the Friedmann equations of both models in the CDM domination era. Both models are then completely constrained by two parameters only, namely  $H_0$  and  $\Omega_m$ , which helps to perform a fair comparison. Therefore, we have:

(i) For  $\Lambda$ CDM, the background evolution reads

$$H(z) = H_0 \sqrt{\Omega_m(1+z)^3 + \Omega_\Lambda},$$

where  $\Omega_\Lambda = 1 - \Omega_m$ . In this case, the Friedmann equation is not sensitive enough to changes in  $\Omega_m$  in order to improve the fit, and  $H_0$  has to adjust to lower values in order to provide for a good fit.

(ii) For  $f(T)$ -CDM, the evolution is given by (3.5), which is more flexible because it invokes *dynamical* torsional dark energy that can be adjusted to accommodate larger  $H_0$  while satisfying all the imposed observational constraints.

Now, as in Fig. 2, we use the different dataset combinations, but combine the 2D joint contours of  $\Lambda$ CDM and  $f(T)$ -CDM in one plot. This is shown in Fig. 5, where we show the  $H_0$ - $\Omega_m$  plane, where  $\Omega_m = \Omega_b + \Omega_c$ . It is apparent that adding the RSD data to the Base dataset, causes the contours of  $\Lambda$ CDM model to shift vertically downwards along the  $H_0$ -axis, while keeping  $\Omega_m$  fixed. On the other hand, the  $f(T)$ -CDM model tends to shift the contours horizontally leftwards along  $\Omega_m$ -axis keeping  $H_0$  fixed. We note that the two parameters  $\Omega_m$  and  $H_0$  are degenerate, whereas the CMB power spectrum constrains the quantity  $\Omega_m h^2$  to a fixed value.

The different interplay in variation of  $H_0$  and  $\Omega_m$  in the two models in fitting the data becomes clearer by considering the concise CMB  $\theta_s$  measurement in the joint likelihood. Again, in the context of  $\Lambda$ CDM the values of  $\Omega_m$  is inflexibly constrained; a good fit requires a lower value of  $H_0$ . In contrast, the  $f(T)$ -CDM model has the freedom to lower the matter density parameter  $\Omega_m$ , while keeping the best-fit value of  $H_0$  large enough to reduce the tension between early and late universe.

#### 5.4 Amplitude of the growth of structure

Another late universe dataset that is in tension with  $\Lambda$ CDM-Planck is the cosmic shear measurements of the matter fluctuation by Kilo Degree Survey 450 (KiDs-450). For the flat  $\Lambda$ CDM model, the matter amplitude  $S_8 = \sigma_8 \sqrt{\Omega_m/0.3} = 0.832 \pm 0.013$  at 68% C.L. as measured by the CMB alone (TT,TE,EE+lowE+lensing) [5]. In contrast, the corresponding value, as measured by KiDs-450 is  $S_8 = 0.745 \pm 0.039$ , when using  $\Lambda$ CDM with a prior on  $H_0$  from direct measurements [17]. This shows that the tension between the early universe measurement of  $S_8$ , as inferred from the CMB and its corresponding late universe measurement, is about  $2.3\sigma$ . Any suggested model to reconcile the early and the late  $H_0$  measurements should not strengthen the tension in other measurements like  $S_8$ .

In Fig. 6, we plot the two dimensional  $S_8$ - $\Omega_m$  plane for both  $\Lambda$ CDM and  $f(T)$ -CDM models using the joint likelihood with/without CMB  $\theta_s$  constraint. It can be seen from that the compilation of the joint datasets does not lead to clear  $S_8$  tension even within the  $\Lambda$ CDM model; it just shows that the 2D contour plots for both models are compatible within  $1\sigma$  regions.

The precise constraint from the early universe, obtained by including the CMB  $\theta_s$  measurement, does not affect the  $S_8$  value of the  $\Lambda$ CDM. On the other hand, the  $f(T)$ -CDM

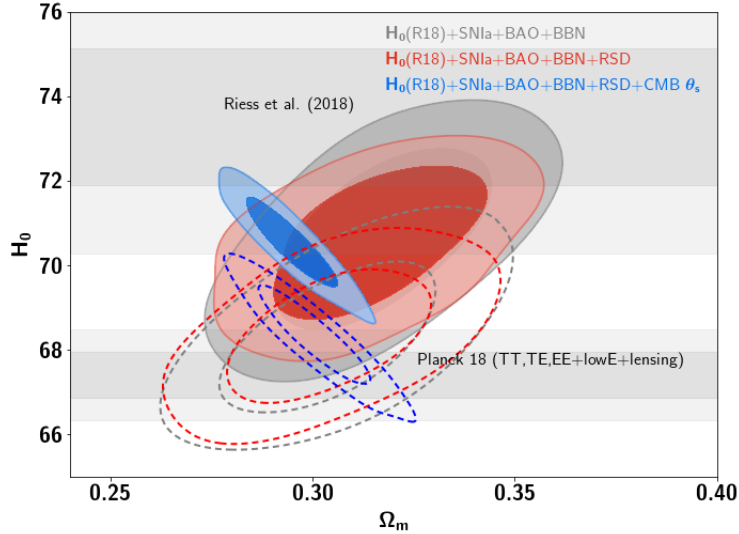


**Figure 5.** Constraints in the  $H_0$ - $\Omega_m$  plane: Solid contours are for the  $f(T)$ -CDM model, while dashed contours are for  $\Lambda$ CDM. The upper grey bands represent  $1\sigma$  and  $2\sigma$  levels of the local measurement of  $H_0$  from R18, while the lower bands represent  $1\sigma$  and  $2\sigma$  of Planck 2018  $H_0$  constraints. As is apparent, when adding the CMB  $\theta_s$  constraint,  $f(T)$ -CDM tends closer to R18  $H_0$  value (which partially alleviates the  $H_0$  tension), while  $\Lambda$ CDM model, as expected, circumscribes  $H_0$  values similar to Planck 2018.

theory predicts similar results with slight tendency to lower the  $S_8$  value by including the CMB  $\theta_s$  constraint. This is also clear from Table 1, which gives the values of  $S_8$  parameter up to 68% C.L. for both models as follows: (i) For  $\Lambda$ CDM, including the CMB  $\theta_s$ , we obtain  $S_8 = 0.782 \pm 0.025$ . (ii) For  $f(T)$ -CDM model, including the CMB  $\theta_s$ , we obtain a lower value  $S_8 = 0.774^{+0.035}_{-0.041}$ . In addition, both predict almost same  $\sigma_8$  values, which indicates that the exponential IR  $f(T)$  gravity does not- in principal- worsen the  $S_8$ -tension.

Optimally, the proper way to test the  $S_8$  tension within the IR  $f(T)$  gravity is to derive its value as inferred by Planck full CMB and KiDs-450 cosmic shear, simultaneously, and then we can properly check their consistency. This requires the extension our analysis to the full linear perturbation effects. As we focus here on testing the viability of the  $f(T)$  model at the background evolution, considering only the effect on the growth of perturbations in terms of modification of background dynamics, we leave such a fuller examination to paper II [46].

In sum, at the background level, we find that the  $f(T)$ -CDM theory (3.1) can fit well with different types of observations. It is statistically similar to  $\Lambda$ CDM and it can serve as a viable theory of gravity, while providing a framework for reducing tensions between early and late universe with  $H_0$  and tentatively does not worsen  $S_8$ . Although, the exponential IR  $f(T)$  theory and  $\Lambda$ CDM are conceptually different, they share the same number of free parameters and are statistically similar in viability in terms of the tests undertaken here.

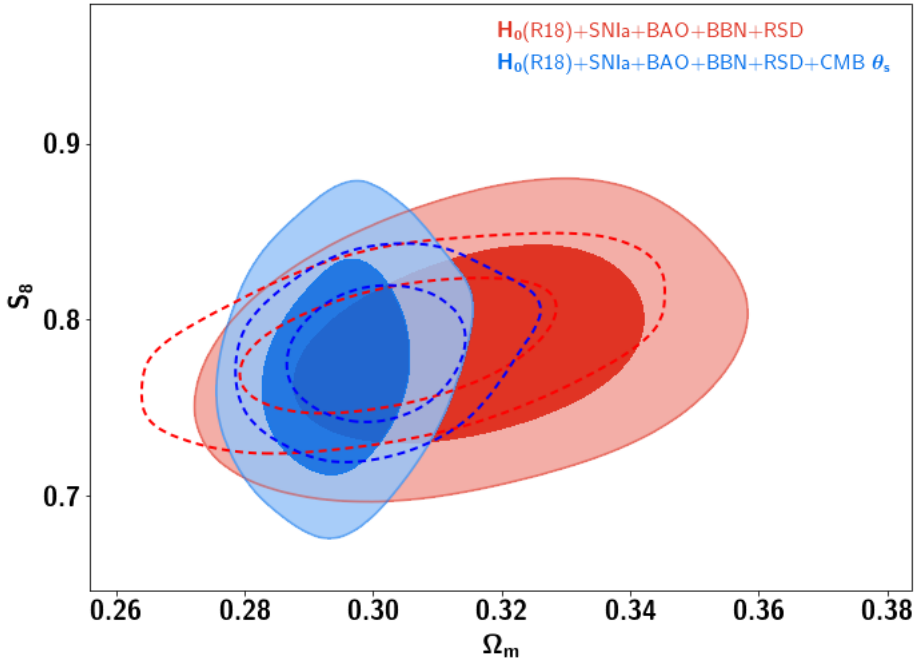


**Figure 6.** Constraints at 68% and 95% CL on  $S_8$ - $\Omega_m$  plane: Solid contours are for  $f(T)$ -CDM model, while dashed contours are for  $\Lambda$ CDM. By including the constraint on the CMB  $\theta_s$  in the likelihood, both models give comparable results. This shows that the exponential IR  $f(T)$  gravity does not worsen  $S_8$  tension in comparison to the  $\Lambda$ CDM model. However, definite conclusion cannot be drawn without performing full linear perturbation of the theory and confronting it with Planck data. This will be investigated in Paper II [46].

## 6 Conclusion

Late accelerated expansion is a crucial issue of unclear origin in contemporary cosmology. The range of possibilities is unconstrained in such a way as to allow for a cosmological constant, dynamical dark energy or modified gravity as sources for the phenomenon. If one assumes the latter option, IR corrections to gravitational theories may represent a viable scenario; as they modify gravity on cosmic distances while keeping GR predictions fulfilled on solar system and smaller distances.

In this context, the exponential IR  $f(T) = Te^{\beta T_0/T}$  gravity was proposed in Ref. [45], its dynamical phase portrait was examined and shown to account for late time acceleration. Here, we examined in detail the empirical viability of the consequence of that model on the background dynamics of cosmic expansion; confronting it with various datasets, covering widely spaced epochs and scales of the Universe.

As the theory does not introduce any extra free parameters compared to  $\Lambda$ CDM, it allows for statistical comparison on equal footing. This is unlike other viable  $f(T)$ , or modified gravity theories in general, which usually include at least one extra free parameter. This being the case, one need not resort to such techniques as performing Bayesian information criteria ( $\text{BIC} = -2 \ln L^{\text{max}} + n \ln m$ ) to obtain well grounded comparisons — since  $n$

(number of parameters) and  $m$  (number of data points) are the same for both models, and only the maximum likelihood  $L^{max}$  (i.e.  $\chi^2_{min}$ ) affects the results. As  $\Lambda$ CDM is already very successful in fitting available data, modified gravity models that improve on those fits by adding tiny modifications through extra parameters are likely to be associated with worse BIC, especially when the number of data points is not so large, c.f. [91]. Furthermore, marginalizing over extra parameters has the effect of enhancing the  $H_0$  tension by broadening the uncertainties of its inferred value rather than an actual shift of the  $H_0$  mean value [30]. Such issues are avoided here.

We used SNIa,  $H_0$ , BAO, RSD, BBN, and CMB  $\theta_s$  to examine the viability of the theory. We evaluated the joint likelihood analysis to find the best-fit values of the four model's parameters  $\{H_0, \Omega_b, \Omega_c, \sigma_8\}$  for both  $\Lambda$ CDM and  $f(T)$ -CDM models. After appropriate modifications of CLASS code with Monte Python, we ran MCMC samples. Then, we used GetDist python package to analyze MCMC chains and get the 2D contour plots at  $1\sigma$  and  $2\sigma$  regions of the different model parameters.

The comparison clearly illustrates that  $f(T)$ -CDM and  $\Lambda$ CDM show similar statistical success when confronted with the various datasets. Moreover, while including the accurate CMB constraint  $\theta_s$ , the  $f(T)$ -CDM theory shows more flexibility, which makes it possible to decrease the  $H_0$  tension by  $1.2\sigma$  relative to the  $\Lambda$ CDM prediction, while still giving an age for the universe ( $\sim 13.76$  Gyr), compatible with other astrophysical observations.

The exponential IR  $f(T)$  gravity considered here drives the effective equation of state to slip significantly into the phantom regime at lower redshifts. Significant deviations from  $\Lambda$ CDM are milder and occur later than those associated with the inverse power-law  $f(T)$  discussed in [43]. This allows the exponential IR  $f(T)$  to be in less severe tension with BAO measurements, in particular the angular distance, while partially alleviating the  $H_0$  tension (by  $\sim 1\sigma$ ). In the present study, this alleviation arose as a compromise statistical optimum fitting the various datasets. Larger tensions with the BAO distances may be expected if full resolution between CMB and local  $H_0$  measurements is required.

The present application of the full dataset does not allow for investigation of the  $S_8$  tension. We limit ourselves to the background evolution and linear matter perturbation in the Newtonian limit, which amounts to modifications of perturbations solely due to the growth rate arising from different background dynamics. The inclusion of the CMB  $\theta_s$  does not affect the  $\Lambda$ CDM prediction of the  $S_8$  value, but with the exponential IR  $f(T)$  theory we find that it leads to slightly lower  $S_8$ , while keeping  $\sigma_8$  almost the same for both models. This indicates that the exponential IR  $f(T)$  gravity does not worsen the  $S_8$  tension. More on such issues calls for extending our analysis of the exponential IR  $f(T)$  gravity to the linear perturbation level, in order to confront it with the full CMB spectra. This we do in paper II.

The IR correction approach is not limited to  $f(T)$  teleparallel gravity, which should be seen as an example of its implications for late acceleration. Although  $f(T)$  cosmology is generally relatively simpler to handle mathematically, other modified gravity models can may successfully explain the late accelerated expansion by weakening the gravity on the cosmic distances as in the case of the IR corrections. A major challenge for  $f(T)$  gravity on the other hand concerns extending its predictions to the non-linear regime of structure

formation, ultimately attempting to adopt it to  $N$ -body simulations, in order to fully test its viability and consequences.

### Acknowledgements

This project was supported financially by the Science and Technology Development Fund (STDF), Egypt. Grant No. 25859. The likelihood analysis presented in this work were done on the Sciama High Performance Compute (HPC) cluster which is supported by the ICG, SEPNet and the University of Portsmouth.

### References

- [1] A.G. Riess, A.V. Filippenko, P. Challis, A. Clocchiatti, A. Diercks, P.M. Garnavich et al., *Observational Evidence from Supernovae for an Accelerating Universe and a Cosmological Constant*, *The Astronomical Journal* **116** (1998) 1009 [[astro-ph/9805201](#)].
- [2] S. Perlmutter, G. Aldering, G. Goldhaber, R.A. Knop, P. Nugent, P.G. Castro et al., *Measurements of  $\Omega$  and  $\Lambda$  from 42 High-Redshift Supernovae*, *Astrophys. J.* **517** (1999) 565 [[astro-ph/9812133](#)].
- [3] S. Weinberg, *The Cosmological Constant Problem*, *Rev. Mod. Phys.* **61** (1989) 1.
- [4] S.M. Carroll, *The Cosmological constant*, *Living Rev. Rel.* **4** (2001) 1 [[astro-ph/0004075](#)].
- [5] PLANCK collaboration, *Planck 2018 results. VI. Cosmological parameters*, [1807.06209](#).
- [6] A.G. Riess, S. Casertano, W. Yuan, L.M. Macri and D. Scolnic, *Large Magellanic Cloud Cepheid Standards Provide a 1% Foundation for the Determination of the Hubble Constant and Stronger Evidence for Physics beyond  $\Lambda$ CDM*, *Astrophys. J.* **876** (2019) 85 [[1903.07603](#)].
- [7] A.G. Riess et al., *A 2.4 Determination of the Local Value of the Hubble Constant*, *Astrophys. J.* **826** (2016) 56 [[1604.01424](#)].
- [8] A.G. Riess, S. Casertano, W. Yuan, L. Macri, J. Anderson, J.W. MacKenty et al., *New Parallaxes of Galactic Cepheids from Spatially Scanning the Hubble Space Telescope: Implications for the Hubble Constant*, *Astrophys. J.* **855** (2018) 136 [[1801.01120](#)].
- [9] A.G. Riess et al., *Milky Way Cepheid Standards for Measuring Cosmic Distances and Application to Gaia DR2: Implications for the Hubble Constant*, *Astrophys. J.* **861** (2018) 126 [[1804.10655](#)].
- [10] DES collaboration, *Dark Energy Survey Year 1 Results: A Precise  $H_0$  Estimate from DES Y1, BAO, and D/H Data*, *Mon. Not. Roy. Astron. Soc.* **480** (2018) 3879 [[1711.00403](#)].
- [11] K.C. Wong et al., *H0LiCOW XIII. A 2.4% measurement of  $H_0$  from lensed quasars: 5.3 $\sigma$  tension between early and late-Universe probes*, [1907.04869](#).
- [12] D. Pesce et al., *The Megamaser Cosmology Project. XIII. Combined Hubble constant constraints*, *Astrophys. J. Lett.* **891** (2020) [[2001.09213](#)].
- [13] C.D. Huang, A.G. Riess, W. Yuan, L.M. Macri, N.L. Zakamska, S. Casertano et al., *Hubble space telescope observations of mira variables in the sn ia host ngc 1559: An alternative candle to measure the hubble constant*, *The Astrophysical Journal* **889** (2020) 5.
- [14] W.L. Freedman, B.F. Madore, D. Hatt, T.J. Hoyt, I.S. Jang, R.L. Beaton et al., *The carnegie-chicago hubble program. viii. an independent determination of the hubble constant based on the tip of the red giant branch*, *The Astrophysical Journal* **882** (2019) 34.

- [15] L. Verde, T. Treu and A.G. Riess, *Tensions between the Early and the Late Universe*, in *Nature Astronomy 2019*, 2019, DOI [1907.10625].
- [16] A.G. Riess, *The Expansion of the Universe is Faster than Expected*, *Nature Rev. Phys.* **2** (2019) 10 [2001.03624].
- [17] H. Hildebrandt et al., *KiDS-450: Cosmological parameter constraints from tomographic weak gravitational lensing*, *Mon. Not. Roy. Astron. Soc.* **465** (2017) 1454 [1606.05338].
- [18] H. Hildebrandt et al., *KiDS+VIKING-450: Cosmic shear tomography with optical and infrared data*, *Astron. Astrophys.* **633** (2020) [1812.06076].
- [19] E. Macaulay, I.K. Wehus and H.K. Eriksen, *Lower Growth Rate from Recent Redshift Space Distortion Measurements than Expected from Planck*, *Phys. Rev. Lett.* **111** (2013) 161301 [1303.6583].
- [20] B.J. Barros, L. Amendola, T. Barreiro and N.J. Nunes, *Coupled quintessence with a  $\Lambda$ CDM background: removing the  $\sigma_8$  tension*, *JCAP* **1901** (2019) 007 [1802.09216].
- [21] A.J. Cuesta, L. Verde, A. Riess and R. Jimenez, *Calibrating the cosmic distance scale ladder: the role of the sound horizon scale and the local expansion rate as distance anchors*, *Mon. Not. Roy. Astron. Soc.* **448** (2015) 3463 [1411.1094].
- [22] P. Lemos, E. Lee, G. Efstathiou and S. Gratton, *Model independent  $H(z)$  reconstruction using the cosmic inverse distance ladder*, *Mon. Not. Roy. Astron. Soc.* **483** (2019) 4803 [1806.06781].
- [23] K. Aylor, M. Joy, L. Knox, M. Millea, S. Raghunathan and W.K. Wu, *Sounds Discordant: Classical Distance Ladder &  $\Lambda$ CDM -based Determinations of the Cosmological Sound Horizon*, *Astrophys. J.* **874** (2019) 4 [1811.00537].
- [24] N. Arendse et al., *Cosmic dissonance: new physics or systematics behind a short sound horizon?*, *Astron. Astrophys.* **639** (2020) [1909.07986].
- [25] R.-Y. Guo, J.-F. Zhang and X. Zhang, *Can the  $H_0$  tension be resolved in extensions to  $\Lambda$ CDM cosmology?*, *JCAP* **02** (2019) 054 [1809.02340].
- [26] E. Di Valentino, A. Melchiorri and J. Silk, *Reconciling Planck with the local value of  $H_0$  in extended parameter space*, *Phys. Lett. B* **761** (2016) 242 [1606.00634].
- [27] E. Di Valentino, A. Melchiorri, E.V. Linder and J. Silk, *Constraining Dark Energy Dynamics in Extended Parameter Space*, *Phys. Rev. D* **96** (2017) 023523 [1704.00762].
- [28] E. Di Valentino, A. Melchiorri and J. Silk, *Cosmological constraints in extended parameter space from the Planck 2018 Legacy release*, *JCAP* **01** (2020) 013 [1908.01391].
- [29] C.D. Kreisch, F.-Y. Cyr-Racine and O. Doré, *Neutrino puzzle: Anomalies, interactions, and cosmological tensions*, *Phys. Rev. D* **101** (2020) 123505 [1902.00534].
- [30] S. Vagnozzi, *New physics in light of the  $H_0$  tension: an alternative view*, 1907.07569.
- [31] V. Poulin, T.L. Smith, T. Karwal and M. Kamionkowski, *Early Dark Energy Can Resolve The Hubble Tension*, *Phys. Rev. Lett.* **122** (2019) 221301 [1811.04083].
- [32] P. Agrawal, F.-Y. Cyr-Racine, D. Pinner and L. Randall, *Rock 'n' Roll Solutions to the Hubble Tension*, 1904.01016.
- [33] J.C. Hill, E. McDonough, M.W. Toomey and S. Alexander, *Early Dark Energy Does Not Restore Cosmological Concordance*, *Phys. Rev. D* **102** (2020) 043507 [2003.07355].

- [34] T.L. Smith, V. Poulin and M.A. Amin, *Oscillating scalar fields and the Hubble tension: a resolution with novel signatures*, *Phys. Rev. D* **101** (2020) 063523 [[1908.06995](#)].
- [35] E. Di Valentino, A. Melchiorri and O. Mena, *Can interacting dark energy solve the  $H_0$  tension?*, *Phys. Rev.* (2017) 043503 [[1704.08342](#)].
- [36] X. Li and A. Shafieloo, *A Simple Phenomenological Emergent Dark Energy Model can Resolve the Hubble Tension*, *Astrophys. J.* **883** (2019) [[1906.08275](#)].
- [37] R.C. Nunes, *Structure formation in  $f(T)$  gravity and a solution for  $H_0$  tension*, *JCAP* **05** (2018) 052 [[1802.02281](#)].
- [38] E. Di Valentino, A. Melchiorri and J. Silk, *Planck evidence for a closed Universe and a possible crisis for cosmology*, *Nat. Astron.* (2019) [[1911.02087](#)].
- [39] E. Di Valentino, A. Melchiorri and J. Silk, *Cosmic Discordance: Planck and luminosity distance data exclude  $\Lambda$ CDM*, [2003.04935](#).
- [40] S.M. Carroll, M. Hoffman and M. Trodden, *Can the dark energy equation - of - state parameter  $w$  be less than -1?*, *Phys. Rev.* (2003) 023509 [[astro-ph/0301273](#)].
- [41] S.M. Carroll, A. De Felice and M. Trodden, *Can we be tricked into thinking that  $w$  is less than -1?*, *Phys. Rev.* (2005) 023525 [[astro-ph/0408081](#)].
- [42] K.J. Ludwick, *The viability of phantom dark energy: A review*, *Mod. Phys. Lett.* (2017) [1730025](#) [[1708.06981](#)].
- [43] A. El-Zant, W. El Hanafy and S. Elgammal,  *$H_0$  Tension and the Phantom Regime: A Case Study in Terms of an Infrared  $f(T)$  Gravity*, *Astrophys. J.* **871** (2019) 210 [[1809.09390](#)].
- [44] S. Nesseris, S. Basilakos, E.N. Saridakis and L. Perivolaropoulos, *Viable  $f(T)$  models are practically indistinguishable from  $\Lambda$ CDM*, *Phys. Rev. D* **88** (2013) 103010 [[1308.6142](#)].
- [45] A. Awad, W. El Hanafy, G.G.L. Nashed and E.N. Saridakis, *Phase Portraits of general  $f(T)$  Cosmology*, *JCAP* **1802** (2018) 052 [[1710.10194](#)].
- [46] M. Hashim et al., *Toward a Concordance Teleparallel Cosmology II. Linear Perturbation*, in progress (2020) .
- [47] R. Aldrovandi and J.G. Pereira, *Teleparallel Gravity*, vol. 173, Springer, Dordrecht (2013), [10.1007/978-94-007-5143-9](#).
- [48] M. Krššák, R. van den Hoogen, J. Pereira, C. Böhmer and A. Coley, *Teleparallel theories of gravity: illuminating a fully invariant approach*, *Class. Quant. Grav.* **36** (2019) 183001 [[1810.12932](#)].
- [49] Y.-F. Cai, S. Capozziello, M. De Laurentis and E.N. Saridakis,  *$f(t)$  teleparallel gravity and cosmology*, *Rept. Prog. Phys.* **79** (2016) 106901 [[1511.07586](#)].
- [50] B. Li, T.P. Sotiriou and J.D. Barrow,  *$f(T)$  gravity and local Lorentz invariance*, *Phys. Rev. D* **83** (2011) 064035 [[1010.1041](#)].
- [51] T.P. Sotiriou, B. Li and J.D. Barrow, *Generalizations of teleparallel gravity and local Lorentz symmetry*, *Phys. Rev. D* **83** (2011) 104030 [[1012.4039](#)].
- [52] M. Krššák and E.N. Saridakis, *The covariant formulation of  $f(T)$  gravity*, *Class. Quant. Grav.* **33** (2016) 115009 [[1510.08432](#)].
- [53] Y.-F. Cai, C. Li, E.N. Saridakis and L. Xue,  *$f(T)$  gravity after GW170817 and GRB170817A*, *Phys. Rev. D* **97** (2018) 103513 [[1801.05827](#)].

- [54] M. Hohmann, M. Krššák, C. Pfeifer and U. Ualikhanova, *Propagation of gravitational waves in teleparallel gravity theories*, *Phys. Rev. D* **98** (2018) 124004 [[1807.04580](#)].
- [55] R. Ferraro and F. Fiorini, *Non trivial frames for  $f(T)$  theories of gravity and beyond*, *Phys. Lett.* (2011) 75 [[1103.0824](#)].
- [56] A. Golovnev, T. Koivisto and M. Sandstad, *On the covariance of teleparallel gravity theories*, *Class. Quant. Grav.* **34** (2017) 145013 [[1701.06271](#)].
- [57] A. Golovnev and T. Koivisto, *Cosmological perturbations in modified teleparallel gravity models*, *JCAP* **1811** (2018) 012 [[1808.05565](#)].
- [58] F.K. Anagnostopoulos, S. Basilakos and E.N. Saridakis, *Bayesian analysis of  $f(T)$  gravity using  $f\sigma_8$  data*, *Phys. Rev. D* **100** (2019) 083517 [[1907.07533](#)].
- [59] L. Amendola et al., *Cosmology and fundamental physics with the Euclid satellite*, *Living Rev. Rel.* **21** (2018) 2 [[1606.00180](#)].
- [60] B. Li, T.P. Sotiriou and J.D. Barrow, *Large-scale structure in  $f(t)$  gravity*, *Phys. Rev. D* **83** (2011) 104017 [[1103.2786](#)].
- [61] G.R. Bengochea and R. Ferraro, *Dark torsion as the cosmic speed-up*, *Phys. Rev. D* **79** (2009) 124019 [[0812.1205](#)].
- [62] E.V. Linder, *Einstein's other gravity and the acceleration of the Universe*, *Phys. Rev. D* **81** (2010) 127301 [[1005.3039](#)].
- [63] K. Bamba, C.-Q. Geng, C.-C. Lee and L.-W. Luo, *Equation of state for dark energy in  $f(T)$  gravity*, *JCAP* **1101** (2011) 021 [[1011.0508](#)].
- [64] SUPERNOVA SEARCH TEAM collaboration, *Observational evidence from supernovae for an accelerating universe and a cosmological constant*, *Astron. J.* **116** (1998) 1009 [[astro-ph/9805201](#)].
- [65] SUPERNOVA COSMOLOGY PROJECT collaboration, *Measurements of  $\Omega$  and  $\Lambda$  from 42 high redshift supernovae*, *Astrophys. J.* **517** (1999) 565 [[astro-ph/9812133](#)].
- [66] D.M. Scolnic et al., *The Complete Light-curve Sample of Spectroscopically Confirmed SNe Ia from Pan-STARRS1 and Cosmological Constraints from the Combined Pantheon Sample*, *Astrophys. J.* **859** (2018) 101 [[1710.00845](#)].
- [67] SDSS collaboration, *Improved Photometric Calibration of the SNLS and the SDSS Supernova Surveys*, *Astron. Astrophys.* **552** (2013) [[1212.4864](#)].
- [68] SDSS collaboration, *Improved cosmological constraints from a joint analysis of the SDSS-II and SNLS supernova samples*, *Astron. Astrophys.* **568** (2014) [[1401.4064](#)].
- [69] J. Mosher et al., *Cosmological Parameter Uncertainties from SALT-II Type Ia Supernova Light Curve Models*, *Astrophys. J.* **793** (2014) 16 [[1401.4065](#)].
- [70] L. Amendola and S. Tsujikawa, *Dark Energy*, Cambridge University Press (2015).
- [71] BOSS collaboration, *The clustering of galaxies in the completed SDSS-III Baryon Oscillation Spectroscopic Survey: cosmological analysis of the DR12 galaxy sample*, *Mon. Not. Roy. Astron. Soc.* **470** (2017) 2617 [[1607.03155](#)].
- [72] BOSS collaboration, *The clustering of galaxies in the completed SDSS-III Baryon Oscillation Spectroscopic Survey: Observational systematics and baryon acoustic oscillations in the correlation function*, *Mon. Not. Roy. Astron. Soc.* **464** (2017) 1168 [[1607.03145](#)].

- [73] BOSS collaboration, *The clustering of galaxies in the completed SDSS-III Baryon Oscillation Spectroscopic Survey: baryon acoustic oscillations in the Fourier space*, *Mon. Not. Roy. Astron. Soc.* **464** (2017) 3409 [[1607.03149](#)].
- [74] M. Vargas-Magaña et al., *The clustering of galaxies in the completed SDSS-III Baryon Oscillation Spectroscopic Survey: theoretical systematics and Baryon Acoustic Oscillations in the galaxy correlation function*, *Mon. Not. Roy. Astron. Soc.* **477** (2018) 1153 [[1610.03506](#)].
- [75] F. Beutler, C. Blake, M. Colless, D.H. Jones, L. Staveley-Smith, L. Campbell et al., *The 6dF Galaxy Survey: baryon acoustic oscillations and the local Hubble constant*, *Mon. Not. Roy. Astron. Soc.* **416** (2011) 3017 [[1106.3366](#)].
- [76] A.J. Ross, L. Samushia, C. Howlett, W.J. Percival, A. Burden and M. Manera, *The clustering of the SDSS DR7 main Galaxy sample – I. A 4 per cent distance measure at  $z = 0.15$* , *Mon. Not. Roy. Astron. Soc.* **449** (2015) 835 [[1409.3242](#)].
- [77] E.A. Kazin et al., *The WiggleZ Dark Energy Survey: improved distance measurements to  $z = 1$  with reconstruction of the baryonic acoustic feature*, *Mon. Not. Roy. Astron. Soc.* **441** (2014) 3524 [[1401.0358](#)].
- [78] Y. Wang et al., *The clustering of the SDSS-IV extended Baryon Oscillation Spectroscopic Survey DR16 luminous red galaxy and emission line galaxy samples: cosmic distance and structure growth measurements using multiple tracers in configuration space*, [2007.09010](#).
- [79] W.J. Percival and M. White, *Testing cosmological structure formation using redshift-space distortions*, *Mon. Not. Roy. Astron. Soc.* **393** (2009) 297 [[0808.0003](#)].
- [80] C. Blake, S. Brough, M. Colless, C. Contreras, W. Couch, S. Croom et al., *The WiggleZ Dark Energy Survey: joint measurements of the expansion and growth history at  $z < 1$* , *Mon. Not. Roy. Astron. Soc.* **425** (2012) 405 [[1204.3674](#)].
- [81] C. Howlett, A. Ross, L. Samushia, W. Percival and M. Manera, *The clustering of the SDSS main galaxy sample – II. Mock galaxy catalogues and a measurement of the growth of structure from redshift space distortions at  $z = 0.15$* , *Mon. Not. Roy. Astron. Soc.* **449** (2015) 848 [[1409.3238](#)].
- [82] F. Beutler, C. Blake, M. Colless, D.H. Jones, L. Staveley-Smith, G.B. Poole et al., *The 6dF Galaxy Survey:  $z \approx 0$  measurements of the growth rate and  $\sigma_8$* , *Mon. Not. Roy. Astron. Soc.* **423** (2012) 3430 [[1204.4725](#)].
- [83] K. Said, M. Colless, C. Magoulas, J.R. Lucey and M.J. Hudson, *Joint analysis of 6dFGS and SDSS peculiar velocities for the growth rate of cosmic structure and tests of gravity*, *Mon. Not. Roy. Astron. Soc.* (2020) [[2007.04993](#)].
- [84] R.J. Cooke, M. Pettini and C.C. Steidel, *One Percent Determination of the Primordial Deuterium Abundance*, *Astrophys. J.* **855** (2018) 102 [[1710.11129](#)].
- [85] D. Blas, J. Lesgourgues and T. Tram, *The Cosmic Linear Anisotropy Solving System (CLASS). Part II: Approximation schemes*, *JCAP* **2011** (2011) 034 [[1104.2933](#)].
- [86] B. Audren, J. Lesgourgues, K. Benabed and S. Prunet, *Conservative constraints on early cosmology with MONTE PYTHON*, *JCAP* **2013** (2013) 001 [[1210.7183](#)].
- [87] A. Lewis, *GetDist: a Python package for analysing Monte Carlo samples*, [1910.13970](#).
- [88] D. Valcin, J.L. Bernal, R. Jimenez, L. Verde and B.D. Wandelt, *Inferring the Age of the Universe with Globular Clusters*, [2007.06594](#).

- [89] K.C. Schlafman, I.B. Thompson and A.R. Casey, *An Ultra Metal-poor Star Near the Hydrogen-burning Limit*, *Astrophys. J.* **867** (2018) 98 [[1811.00549](#)].
- [90] R. Jimenez, A. Cimatti, L. Verde, M. Moresco and B. Wandelt, *The local and distant Universe: stellar ages and  $H_0$* , *JCAP* **03** (2019) 043 [[1902.07081](#)].
- [91] B. Xu, H. Yu and P. Wu, *Testing Viable  $f(T)$  Models with Current Observations*, *Astrophys. J.* **855** (2018) 89.